Journal of Electrical and Computer Engineering Innovations
(JECEI)
Journal homepage: http://www.jecei.sru.ac.ir

Research paper

Bidirectional Buck-Boost Integrated Converter for Plug-in Hybrid Electric Vehicles

H. Soltani Gohari**, K. Abbaszadeh
Department of Electrical Engineering, K.N.Toosi University of Technology, Tehran, Iran.

Article Info

Article History:
Received 19 February 2019
Reviewed 27 April 2019
Revised 05 May 2019
Accepted 02 December 2019

Keywords:
Plug-in hybrid EV
On-board charger
DC-DC converter
Regenerative braking
Vehicle-to-grid

*Corresponding Author's Email Address:
Hsoltani@email.kntu.ac.ir

Abstract

Background and Objectives: Power electronics infrastructures play an important role in charging different types of electric vehicles (EVs) especially Plug-in Hybrid EVs (PHEVs). Designing appropriate power converters is the topic of various studies.
Method: In this paper, a novel bidirectional buck-boost multifunctional integrated converter is presented which is capable of handling battery and fuel cell stack in plug-in hybrid electric vehicles. The proposed converter has the ability to work in five different operating modes (Charging/Propulsion (only battery)/ Propulsion (battery and FC)/ Regenerative braking/ V2G). The introduced multifunctional two-stage converter has the ability to work in all the above-mentioned modes in buck- boost condition, the feature that does not exist in the previous works. It is possible to control active and reactive power by using the effective dual-loop PI control method which is introduced in this paper. Working as an on-board charger and DC-DC converter (which interfaced between power sources and motor drive system) causes a decrease in the counts of the total components and an increase in system efficiency.
Results: Operation principle and steady-state analysis of each stage of the proposed converter in all operating modes are provided in detail and in order to design an appropriate applicable converter, the design considerations and procedure are also explained for capacitive and inductive components. The proposed converter is simulated in MATLAB/SIMULAIN environment and results are provided. Voltage and current waveforms in all operating conditions are provided with their transient. FFT analysis of the input current (in the operating modes in which the converter absorb or deliver power from/to the grid) is also mentioned. A reduced-scale setup of the presented converter is built and tested and experimental results confirm simulation ones.
Conclusion: A bidirectional buck-boost integrated converter in PHEVs applications is introduced in this paper. The design procedure of the presented converter is provided and also an effective control method to control active and reactive power during charging and V2G modes is introduced. A comparison study of the proposed converter with other similar converters introduced in recent years in terms of the number of high-frequency switches in each mode is also done. Simulation and experimental results are also provided.

Introduction

Different attempts to find practical solutions for increasing environmental problems during recent years have caused significant developments in different types of electric vehicles [1], [2].

Fully electric vehicles (EVs) or plug-in EVs (PEVs) and hybrid electric vehicles (HEVs) or plug-in hybrid EVs (PHEVs) are the main categories of non-fossil fuels vehicles. There are some limitations in using the PEVs, which receive their energy entirely from the electricity grid because of their battery pack, which is used to store needed energy such as performance degradation because of high current dischargers and low life [3], [4]. Hybridization of EVs' powertrain, which leads to the plug-in hybrid electric vehicles (PHEVs), is a beneficial solution for battery pack challenges that usually is done by adding fuel cell stack to the power train. Additionally, PHEVs do not have disadvantages of the fuel cell vehicles (FCVs), which receive their needed power entirely from FC stacks, such as slow transient response and degradation effects. Multi-source powertrains need special DC-DC converters, which are interfaced between the power sources and motor drive system [5]-[7]. Working in battery charging, regenerative braking, and propulsion (battery discharging) operating modes intensifies the need for a bidirectional converter on the battery side. On the other hand, using charge equalizer circuits (CECs) causes the battery port voltage to change over a wide range by bypassing and adding battery cells according to their state of charge (SOC). In addition, the induced voltage of the motor changes in a wide range during regenerative braking, depending on the car speed. So the bidirectional DC-DC converter adopted on the battery side should be able to work as a buck-boost converter in both directions.

In addition to the above-mentioned DC-DC converter, an AC-DC converter is also required in charging (charging the battery with the AC grid voltage) and discharging (V2G) modes. Exploiting an appropriate bidirectional buck-boost converter enables the PHEV to be charged and discharged by universal voltage supply (90-260V [8], [9]) and improves the input current waveform by making it feasible to select the DC-link voltage of the AC-DC converter in a wide range.

In conventional powertrains, two separated converters are utilized for charging and propulsion modes. This fact increases the entire system losses and decreases system reliability. A very effective way to improve system reliability and efficiency is to merge these converters. This integration enables the designer to utilize different components, especially semiconductor devices and passive components, in more than one operating mode, so the components' count can be reduced. This integrated converter should have all the features mentioned above in addition to the ability to manage the used energy of each power source.

In [10], a bidirectional DC-DC converter is proposed, which can be used in PEVs as the converter interfaced between the energy storage system (ESS) and the motor drive system. Although it has high voltage ratio and low voltage stress on semiconductor devices, it cannot work as a buck-boost converter in both directions and also needs extra circuits for charging the battery and handling other power sources. In [11], a bidirectional DC-DC converter with a wide voltage gain ratio is presented. In addition to its disability to increase and decrease voltage level in both directions, one converter is needed for each power source in PHEVs, so the entire system efficiency and reliability can be decreased because of the components numbers. The DC-DC converters proposed in [12], [13] are capable of handling more than one power source in PHEVs. The converter introduced in [12] cannot work in regenerative braking mode and is able to work only as a boost converter. Although the converter considered in [13] has the ability to return the regenerative braking energy to the battery, it cannot act as a buck-boost converter in different modes. Authors in [14], [15] have proposed two multi-port bidirectional DC-DC converters that are suitable for hybrid powertrains and work in different operating modes, which is an outstanding feature, but an extra charger circuit is needed to charge the battery by the grid. The integrated converters proposed in [16], [17] can work in charging and propulsion modes. Although the converter proposed in [16] can increase/decrease the voltage in propulsion and regenerative braking modes, it is not suitable for PHEVs, which have more than one power source and cannot work in V2G mode. The converter presented in [17] is an efficient reduced-part integrated converter that can used in the BEVs. The main drawback of the proposed converter is that it can only work in the charging mode when the battery voltage is higher than the peak of the grid voltage. Additionally, it is not suitable for PHEVs and cannot work in V2G mode. The integrated charger introduced in [18] is applicable in PEVs with one power source and can work in the buck-boost condition in charging mode only. A very high performance integrated converter is considered in [19], which can work in charging, propulsion, and regenerative braking modes, but it is not suitable for PHEVs. The switching bidirectional buck-boost converter presented in [20] is suitable for the Li-battery/super-capacitor hybrid ESS of EVs, which can only work in charging and V2G modes and needs extra circuits for handling propulsion and regenerative braking modes.

Introducing an appropriate integrated converter suitable for PHEVs, which is capable of doing all the aforementioned tasks (battery charging by grid, hybrid propulsion, regenerative braking, and vehicle to grid) in the buck-boost condition (in all operating modes), the feature that is not exist in the reviewed converters, is the motivation of this work.

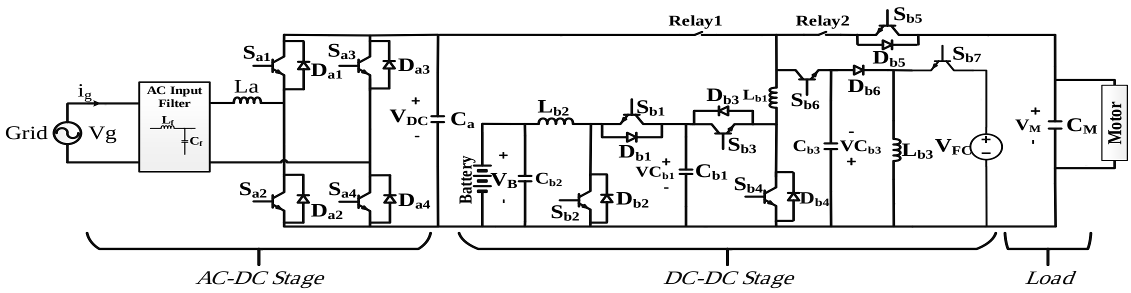

Fig. 1: Topology of proposed converter.

In this paper a bidirectional buck-boost integrated converter is presented which is capable of handling battery and FC stack in PHEVs. The presented converter has the ability to work in five operating modes and paly the roles of an on-board bidirectional buck-boost charger and a bidirectional DC-DC converter, which interfaced between power sources and motor drive system, without any need for additional power circuit. An effective control method is also explained which enables the proposed converter to control active and reactive power during charging and V2G modes and improves input current waveform in terms of total harmonic distortion (THD).

Proposed Converter; System Description and Analysis

Topology and Modes of Operation

Fig. 1 shows the topology of the proposed converter, where V_g, V_B, V_{FC}, and V_M represent the grid voltage, battery port voltage, fuel cell stack output voltage, and DC-link of motor drive system voltage, respectively. The presented converter structure can be divided into two stages. First stage: a bidirectional AC-DC converter which can work as a controllable rectifier and inerter in each direction. Second stage: a four-port DC-DC converter which can be controlled according to the converter operating mode. As shown in

Fig. 2, the proposed converter has the ability to work in five different operating modes:

1- Mode1 (Battery charging from the grid): in this mode the battery of PHEV is charged by the grid with controllable active and reactive power and pure sinusoidal input current waveform. The ability to increase and decrease the voltage on the battery side enables the proposed converter to be used in the PHEVs with wide range of battery voltage and be charged with universal voltage supply.

2- Mode2 (Propulsion; Only Battery): when the EV starts accelerating or when FC stack is not able to work because of the slow dynamic response of FC stack or its efficiency problems, the PHEV can receive its needed power from the battery by working the proposed converter in the second mode.

3- Mode3 (Propulsion; FC and Battery): when the converter is operated in this mode, both battery and FC provide the needed power. The capability of working in buck-boost condition enables the central control unit to manage energy of each power source better.

4- Mode4 (Regenerative braking): during EV braking condition, the energy of regenerative braking can be returned and stored in the battery. During different braking conditions with different speeds and different induced voltage levels, the returning energy process can be done properly because of the buck-boost structure of the proposed converter.

5- Mode5 (Vehicle-to-Grid (V2G)): the ability to work in this mode enables the PHEVs to handle V2G mode and return their surplus energy to the grid with controllable active and reactive power according to the commands of the smart grid or costumer.

As mentioned above, the proposed converter operates in five operating modes depending on the vehicle and power sources' conditions. As long as the vehicle is parked and connected to the grid the relay1 is ON and relay2 is OFF and converter works in charging and V2G modes (Mode1 and Mode5). When the vehicle is disconnected from the grid and is used by driver the relay1 is turned OFF and relay2 is turned ON and converter is allowed to work in propulsion and regenerative braking modes.

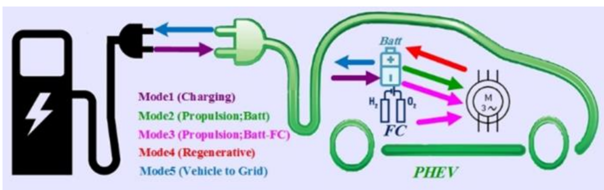

Fig. 2: Operating modes of proposed converter.

Operation Principle and Steady State Analysis

A. Mode1: Charging battery by grid

In this operating mode, the battery of the connected PHEV is charged by utility grid. Because of the ability of converter to work as buck-boost converter in this mode, various battery packs with wide range of voltage can be charged by a wide range of utility grid. Additionally the controlling active and reactive power and input current waveform can be done better. The first stage rectifies and boosts the grid voltage and charges the DC-link capacitor (C_a). Then the DC-DC stage regulates the voltage level and charges the battery.

➢ **AC-DC Stage**

The first stage should control active and reactive power and input current waveform which can be done by the different control methods and switching patterns. In this paper a high efficiency and low conducting loss switching method explained in [21] and the effective control method introduced in "Control Method" section are adopted for the AC-DC stage. The proposed switching method controls the switches Sa1 and Sa2 depending on the sign of the grid voltage. It is worth mentioning that the switches Sa3 and Sa4 are OFF in this mode.

Vg>0: when the grid voltage is in its positive half-cycle, the Sa2 has high frequency operation and Sa1 is OFF.

State1 (0<t<DTs): as shown in Fig. 3 (a), in this state Sa2 is ON and L_a is magnetized via utility grid (V_g).

State2 (DTs<t<Ts): at t=DTs Sa2 is turned OFF and L_a is demagnetized with (V_g-V_{DC}) so C_a is charged [Fig. 3(b)].

Vg<0: in this condition Sa1 has high frequency operation.

State1 (0<t<DTs): in this state Sa1 is ON and L_a is magnetized via utility grid [Fig. 3(c)].

State2 (DTs<t<Ts): in this state Sa1 is in OFF-state and L_a is demagnetized so C_a is charged [Fig. 3(d)].

In order to calculate the voltage gain of the AC-DC stage the operation of this stage in the positive half-cycle of grid voltage should be analyzed. As shown in Fig. 3(a), the voltage of the L_a in the first state is obtained as:

$$\begin{cases} V_{La} = V_g & 0 < t < DT_s \\ V_{La} = V_g - V_{DC} & DT_s < t < T_s \end{cases} \tag{1}$$

The volt-sec balance of this inductor can be written as:

$$\langle i_{La} \rangle = 0 \rightarrow \frac{1}{T_s}\left[\int_0^{DTs} (V_g) dt + \int_{DTs}^{Ts} (V_g - V_{DC}) dt\right] = 0 \tag{2}$$

By solving above equation the voltage gain of boost rectifier can be achieved as (3):

$$\frac{V_{DC}}{V_g} = \frac{1}{1-D} \tag{3}$$

➢ **DC-DC Stage**

In this mode the DC-DC stage charges the battery by controlling Sb1 and Sb4. The operation of this stage is divided into two states in this mode.

State1 (0<t<DTs): in this time interval Sb1 and Sb4 are ON so L_{b1} and L_{b2} are magnetized by (V_{DC}) and (V_{Cb1}-V_B), respectively. The energy of capacitor C_{b1} is released to L_{b2} so C_{b1} is discharged [Fig. 4(a)].

State2 (DTs<t<Ts): at t=DTs the both Sb1 and Sb4 are turned OFF so anti-parallel diodes D_{b2} and D_{b3} are forward-biased. As a result L_{b1} and L_{b2} are demagnetized by (V_{DC}-V_{Cb1}) and (-V_B), respectively. C_{b1} is charged in this state [Fig. 4 (b)].

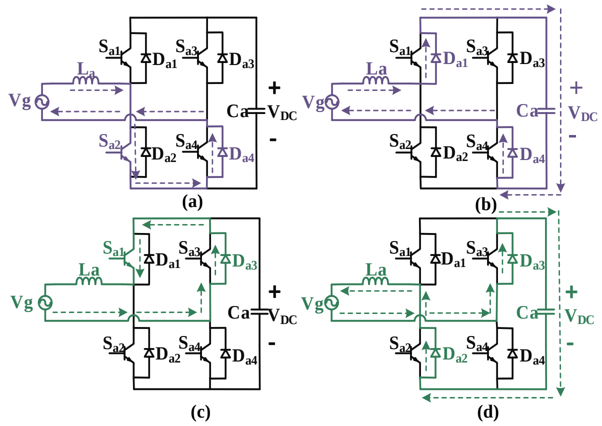

Fig. 3: Current paths of AC-DC stage in mode1.

As mentioned above, voltage across Lb1 and Lb2 are:
For 0<t<DTs:

$$\begin{cases} V_{Lb1} = V_{DC} \\ V_{Lb2} = V_{Cb1} - V_B \end{cases} \tag{4}$$

and for DTs<t<Ts:

$$\begin{cases} V_{Lb1} = V_{DC} - V_{Cb1} \\ V_{Lb2} = -V_B \end{cases} \tag{5}$$

So the volt-sec principle for each inductor can be written as:

$$\langle i_{Lb1} \rangle = 0 \rightarrow \frac{1}{T_s}\left[\int_0^{DTs} (V_{DC}) dt + \int_{DTs}^{Ts} (V_{DC} - V_{Cb1}) dt\right] = 0 \tag{6}$$

$$\langle i_{Lb2} \rangle = 0 \rightarrow \frac{1}{T_s}\left[\int_0^{DTs} (V_{Cb1} - V_B) dt + \int_{DTs}^{Ts} (-V_B) dt\right] = 0 \tag{7}$$

By solving above equations, the volt-sec balance can be rewritten as:

$$D(V_{DC}) + (1-D)(V_{DC} - V_{Cb1}) = 0 \tag{8}$$

$$D(V_{Cb1} - V_B) + (1-D)(-V_B) = 0 \tag{9}$$

By manipulating (8), the voltage of Cb1 can be found as yields:

$$V_{Cb1} = \frac{1}{1-D} V_{DC} \tag{10}$$

Substituting (10) into (9) leads to obtaining the ideal voltage gain of mode1 as:

$$\frac{V_B}{V_{DC}} = \frac{D}{1-D} \tag{11}$$

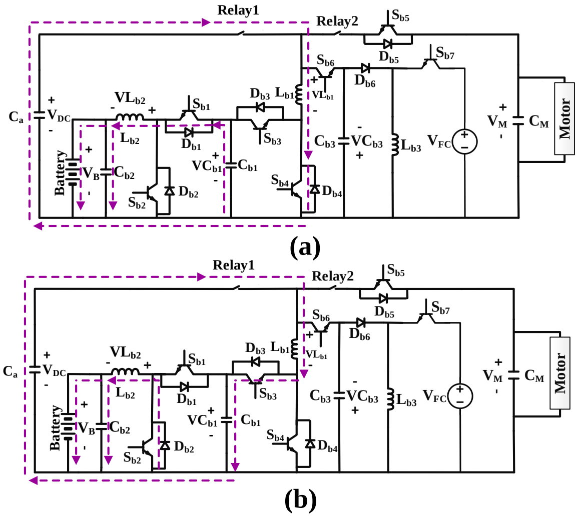

Fig. 4: Current paths of DC-DC stage in mode1.

B. *Mode2: Propulsion (Battery)*

In this operating mode the battery is supplying the energy to the motor drive system so the first stage does not have any task in this mode. For this purpose the relay1 is OFF and relay2 is in ON-state. The DC-DC stage operates as follows:

State1 (0<t<DTs): at first Sb2 and Sb3 are turned ON, simultaneously, so anti-parallel diodes D_{b1} and D_{b4} are reverse biased. As a result, L_{b1} and L_{b2} are magnetized with (V_{Cb1}-V_M) and V_B, respectively [Fig. 5 (a)].

State2 (DTs<t<Ts): in this state all switches of DC-DC stage are turned OFF so anti-parallel diodes Db1 and Db2 are forward-biased. In this condition L_{b1} and L_{b2} are demagnetized with (-V_M) and (V_B-V_{Cb1}), respectively [Fig. 5 (b)].

As shown in Fig. 5, the voltage across inductors L_{b1} and L_{b2} can be written as:

For 0<t<DTs:

$$\begin{cases} V_{Lb1} = V_{Cb1} - V_M \\ V_{Lb2} = V_B \end{cases} \tag{12}$$

and for DTs<t<Ts:

$$\begin{cases} V_{Lb1} = -V_M \\ V_{Lb2} = V_B - V_{Cb1} \end{cases} \tag{13}$$

So the zero average inductors voltages over one switching cycle are:

$$\langle i_{Lb1} \rangle = 0 \rightarrow \frac{1}{T_s}\left[\int_0^{DTs}(V_{Cb1} - V_M)dt + \int_{DTs}^{Ts}(-V_M)\,dt\right] = 0 \tag{14}$$

$$\langle i_{Lb2} \rangle = 0 \rightarrow \frac{1}{T_s}\left[\int_0^{DTs}(V_B)dt + \int_{DTs}^{Ts}(V_B - V_{Cb1})\,dt\right] = 0 \tag{15}$$

Solving above equations leads to:

$$D(V_{Cb1} - V_M) + (1-D)(-V_M) = 0 \tag{16}$$

$$D(V_B) + (1-D)(V_B - V_{Cb1}) = 0 \tag{17}$$

From (16) the voltage of C_{b1} can be obtained as:

$$V_{Cb1} = DV_M \tag{18}$$

By substituting (18) into (17), the ideal voltage gain of mode2 is obtained as:

$$\frac{V_M}{V_B} = \frac{D}{1-D} \tag{19}$$

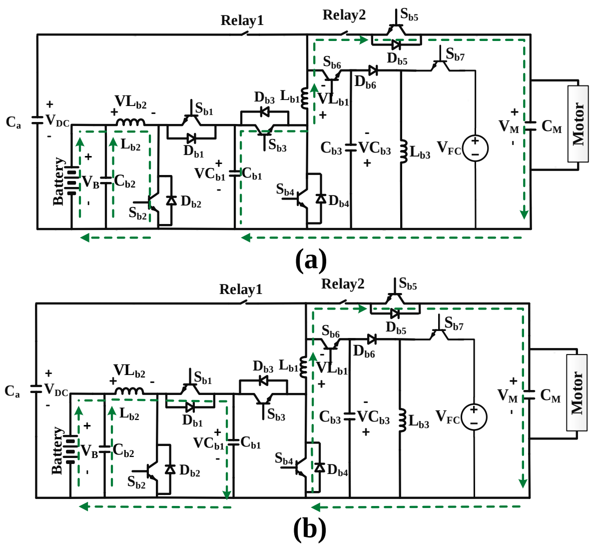

Fig. 5: Current paths of DC-DC stage in mode2.

C. *Mode3: Propulsion (Battery + Fuel cell)*

When the fuel cell stack has the ability to participate in providing needed energy, the central control system sends Sb6 and Sb7 gate signals and converter delivers the energy of the battery and fuel cell to the motor drive system, simultaneously. Fig. 6 shows the operation principle of the converter in this mode. Because of the converter ability to regulate battery voltage in wide range, the battery cells with less SOCs can be bypassed in order to equalize discharging process.

State1 (0<t<DTs): this state begins when the Sb6 and Sb7 receive gate signals. In this state Sb2, Sb3, Sb6 and Sb7 are turned ON. The Db5 is reverse biased so L_{b1} is magnetized by C_{b1} and C_{b3} which are charged in the previous time interval. L_{b2} and L_{b3} are also magnetized by (V_B) and (V_{FC}), respectively [Fig. 6 (a)].

State2 (DTs<t<Ts): during this state, all switches of the DC-DC stage are turned OFF so diodes D_{b1}, D_{b4}, D_{b5}, and D_{b6} are forward-biased. In this condition L_{b1} and L_{b2} are demagnetized by (-V_M) and (V_B-V_{Cb1}), respectively. The C_{b3} starts charging through L_{b3} which is magnetized in previous state [Fig. 6 (b)].

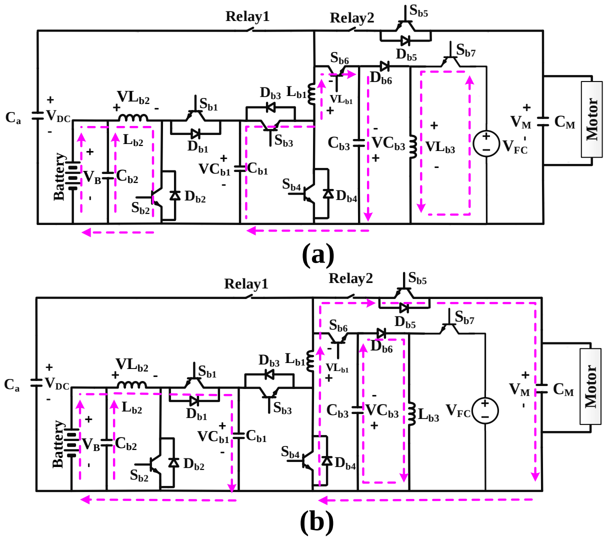

Fig. 6: Current paths of DC-DC stage in mode3.

By using KVL, the voltage across inductors in each state are obtained as:

For 0<t<DTs:

$$\begin{cases} V_{Lb1} = V_{Cb1} + V_{Cb3} \\ V_{Lb2} = V_B \\ V_{Lb3} = V_{FC} \end{cases} \tag{20}$$

and for DTs<t<Ts:

$$\begin{cases} V_{Lb1} = -V_M \\ V_{Lb2} = V_B - V_{Cb1} \\ V_{Lb3} = -V_{Cb3} \end{cases} \tag{21}$$

The volt-sec balance can be written as:

$$\langle i_{Lb1} \rangle = 0 \rightarrow \frac{1}{T_s}\left[\int_0^{DTs} (V_{Cb1} + V_{Cb3})dt + \int_{DTs}^{Ts} (-V_M)\,dt\right] = 0 \tag{22}$$

$$\langle i_{Lb2} \rangle = 0 \rightarrow \frac{1}{T_s}\left[\int_0^{DTs} (V_B)dt + \int_{DTs}^{Ts} (V_B - V_{Cb1})\,dt\right] = 0 \tag{23}$$

$$\langle i_{Lb3} \rangle = 0 \rightarrow \frac{1}{T_s}\left[\int_0^{DTs} (V_{FC})dt + \int_{DTs}^{Ts} (-V_{Cb3})\,dt\right] = 0 \tag{24}$$

Solving above equations leads to:

$$D(V_{Cb1} + V_{Cb3}) + (1-D)(-V_M) = 0 \tag{25}$$

$$D(V_B) + (1-D)(V_B - V_{Cb1}) = 0 \tag{26}$$

$$D(V_{FC}) + (1-D)(-V_{Cb3}) = 0 \tag{27}$$

From (26) the voltage of C_{b1} can be obtained as:

$$V_{Cb1} = \frac{1}{1-D} V_B \tag{28}$$

and From (27) the voltage of Cb3 can be obtained as:

$$V_{Cb3} = \frac{D}{1-D} V_{FC} \tag{29}$$

By substituting (28) and (29) into (25) the voltage of motor drive system can be calculated as:

$$V_M = \frac{D^2}{(1-D)^2} V_{FC} + \frac{D}{(1-D)^2} V_B \tag{30}$$

D. Mode4: Regenerative Braking

As soon as the vehicle brakes, the switch Sb5 is turned ON and Sb6 and Sb7 are turned OFF so the energy flows from motor drive system to the battery. Due to the buck-boost structure of the converter, the energy returning process can be done properly with a wide variation of the vehicle speed.

State1 (0<t<DTs): during this state Sb1, Sb4, and Sb5 are in ON-state so L_{b1} and L_{b2} are magnetized by (V_M) and ($V_{Cb1} - V_B$), respectively [Fig. 8(a)].

State2 (DTs<t<Ts): in this time interval all switches are turned OFF except Sb5 so Db2 and Db3 are direct biased. In this condition L_{b1} and L_{b2} are demagnetized by (V_M-V_{Cb1}) and (-V_B), respectively, and C_{b1} starts charging [Fig. 8(b)].

The same approach as the mode1 can be used for calculating voltage gain of mode4. The volt-sec principle can be written as:

$$\langle i_{Lb1} \rangle = 0 \rightarrow \frac{1}{T_s}\left[\int_0^{DTs} (V_M)dt + \int_{DTs}^{Ts} (V_M - V_{Cb1})\,dt\right] = 0 \tag{31}$$

$$\langle i_{Lb2} \rangle = 0 \rightarrow \frac{1}{T_s}\left[\int_0^{DTs} (V_{Cb1} - V_B)dt + \int_{DTs}^{Ts} (-V_B)\,dt\right] = 0 \tag{32}$$

By solving above equations, similar to mode1, the voltage gain of mode4 is obtain as:

$$\frac{V_B}{V_M} = \frac{D}{1-D} \tag{33}$$

E. Mode 5: Vehicle to Grid

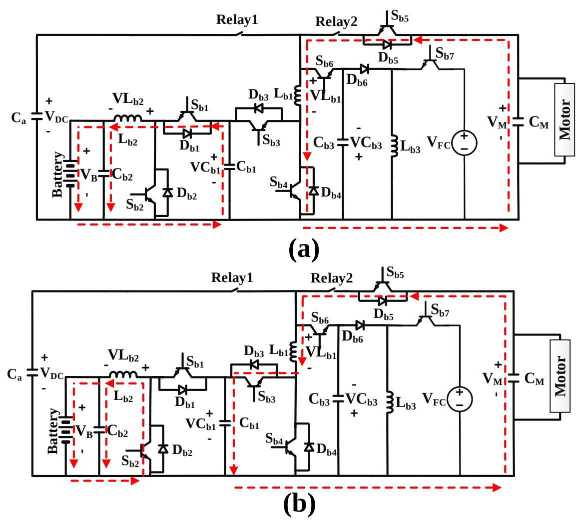

Fig. 7: Current paths of DC-DC stage in mode4.

It is possible to return surplus EV energy to grid for different reasons by operating the proposed converter in the mode5. Peak shaving is a very important task which can be done by using electric vehicles as mobile power sources. The proposed converter can return parked EV's energy to utility grid by controllable active and reactive power according to the processed commands of smart grid or customer. At first the DC-DC stage increase or decrease the voltage of battery according to the DC-link voltage reference and then the AC-DC stage works as single-phase full-bridge inverter and delivers the energy of DC-link capacitor to the grid.

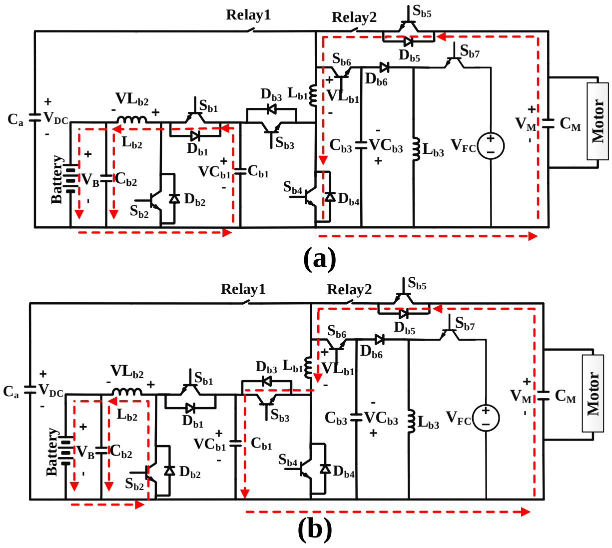

Fig. 8: Current paths of DC-DC stage in mode4

➢ AC-DC Stage

In order to invert the DC voltage of DC-link into AC, the AC-DC stage uses the switching pattern which is explained in [21] and detailed here. Similar to the mode1, the operation of this stage depends on the sign of the voltage grid as follows:

Vg>0: in this condition, during first state (0<t<DTs) Sa1 and Sa4 are turned ON so the L_a is magnetized with (V_{DC}-V_g) [Fig. 9 (a)]. In the next state (DTs<t<Ts) the Sa1 is turned OFF and L_a demagnetized via Da2 and Sa4 [Fig. 9 (b)].

Vg<0: when V_g is in its negative half-cycle, Sa2 has high frequency operation and Sa3 operates with grid frequency. This switching pattern causes L_a to magnetize and demagnetize as shown in Fig. 9 (c)-(d).

Using the same approach as the mode1, the voltage gain of AC-DC stage can be calculated in this mode. The voltage across L_a can be written as follows:

$$\begin{cases} V_{La} = V_{DC} - V_g & 0 < t < DT_s \\ V_{La} = -V_g & DT_s < t < T_s \end{cases} \tag{34}$$

By applying the volt-sec balance law, the voltage gain of buck inverter can be achieved as (35):

$$\frac{V_g}{V_{DC}} = D \tag{35}$$

➢ DC-DC Stage

As mentioned above, since the vehicle is connected to grid relay1 is ON and relay2 is OFF. Operation of the converter in this mode is divided into two states:

State1 (0<t<DTs): as depicted in Fig. 10 (a), in this state Sb2 and Sb3 are in ON-state so L_{b1} and L_{b2} are magnetized by (V_{Cb1}-V_{DC}) and (V_B), respectively.

State2 (DTs<t<Ts): by turning OFF both Sb2 and Sb3, the C_{b1} starts charging through the charged inductor (L_{b2}) so L_{b2} demagnetized by (V_B-V_{Cb1}). The L_{b1} is also demagnetized by (-V_{DC}) [Fig. 10 (b)].

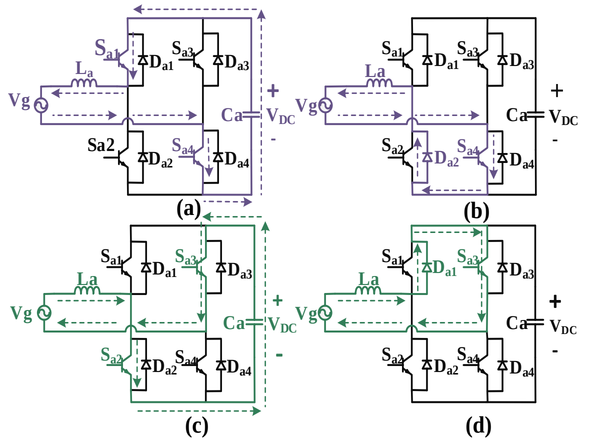

Fig. 9: Current paths of AC-DC stage in mode5.

In this mode, the volt-sec balance can be written as:

$$\langle i_{Lb1} \rangle = 0 \rightarrow \frac{1}{T_s}\left[\int_0^{DTs} (V_{Cb1} - V_{DC}) dt + \int_{DTs}^{Ts} (-V_{DC})\, dt\right] = 0 \tag{36}$$

$$\langle i_{Lb2} \rangle = 0 \rightarrow \frac{1}{T_s}\left[\int_0^{DTs} (V_B) dt + \int_{DTs}^{Ts} (V_B - V_{Cb1})\, dt\right] = 0 \tag{37}$$

By using same approach as mode2, the voltage gain of mode5 can be obtained as:

$$\frac{V_{DC}}{V_B} = \frac{D}{1-D} \tag{38}$$

As studied in (11), (19), (30), (33), and (38), the converter works as a buck-boost which is an outstanding feature of that.

Design Considerations

The design considerations and procedure of inductive and capacitive components of proposed converter are detailed in this section. The total value of the inductive component of the AC input filter can be obtained as:

$$L_f = L_{req} + L_g \tag{39}$$

where L_{req} is the value of the required inductor which should be added and L_g is the grid impedance which is considered 4-5% of the base impedance [22]. So the value of the required inductor that should be added to circuit can be calculated as:

$$L_{req}=\frac{1}{4\pi^2 f_c^{\,2} C_f}-4\times10^{-2}\times\left[\frac{1}{\omega_L}\right]\times\left[\frac{V_g^{\,2}}{P_{out}}\right] \quad (40)$$

where f_c is the cut-off frequency. Maximum value of the capacitive component of the filter can be calculate as [23]:

$$C_{f\,\max}=\frac{I_m}{\omega V_m}\tan(\theta)=\frac{\sqrt{2}P_{\max}}{\omega_L V_m V_g}\tan(\theta) \quad (41)$$

where, V_m, I_m, and θ are the peak value of grid voltage, peak value of input current, and displacement angle between grid voltage and input current, respectively.

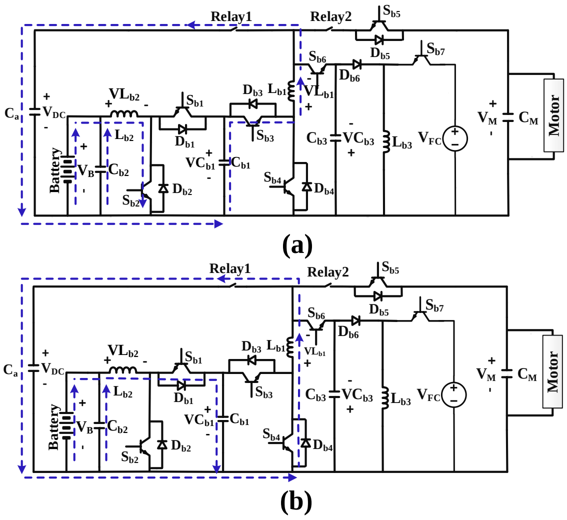

Fig. 10: Current paths of DC-DC stage in mode5

Reaching to a proper input current waveform entirely depends on the values of the inductor and capacitor of the AC-DC stage (L_a and C_a). In order to calculate minimum value of the inductor the magnetizing time of that should be analyzed. The voltage of L_a can be written as:

$$V_{La}=L_a\frac{di_{La}}{dt}\rightarrow V_{La}=L_a\frac{\Delta i_{La}}{\Delta t}\xrightarrow[\Delta t=DTs]{\Delta i_{La}=\Delta ig}$$
$$\Delta i_g=\frac{V_{La}*DTs}{L_a} \quad (42)$$

As shown in Fig. 3 (a), in the magnetizing time the voltage of L_a can be written as:

$$V_{La}=V_g \quad (43)$$

And as calculated in (3), the grid voltage can be rewritten as follows:

$$V_g=(1-D)*V_{DC} \quad (44)$$

By substituting (43) and (44) into (42) and manipulating it, the value of the L_a is obtained as:

$$L_a=\frac{V_{DC}*D*(1-D)}{\Delta i_g*f_s} \quad (45)$$

where f_s is the switching frequency. The worst case occurred in the maximum value of the D(1-D) term which is equal to 0.25 so:

$$L_a=\frac{V_{DC}}{4*\Delta i_g*f_s} \quad (46)$$

Using an appropriate capacitor in the DC-link is the only way to deliver constant power to the battery by the single-phase grid. The value of this component affects the ripple of the voltage and current of the battery during charging mode. So it should be designed properly. The instantaneous power of the grid can be written as:

$$p(t)=V*I*\cos\varphi+2*V*I*\cos(2\omega t+\varphi) \quad (47)$$

which consists of an average and oscillating value of the power, respectively. The oscillating term affects the oscillating voltage amplitude of the DC-link voltage (Δv_{DC}) so:

$$\frac{1}{2}\cdot C_a\cdot v_{DC}^{\,2}=\int\tilde{p}dt \quad (48)$$

By substituting oscillating term of (47) into (48), the required value of C_a is obtained as:

$$C_a=\frac{2V_gI_g}{\omega\Delta v_{DC}V_{DC}} \quad (49)$$

Designing the L_{b1} and L_{b2} can be done similar to the L_a. For both inductors the below general equation can be used:

$$V_L=L\frac{di_L}{dt}\rightarrow V_L=L\frac{\Delta i_L}{\Delta t} \quad (50)$$

Since each inductor have different voltages in each mode, all modes should be considered and the worst case should be selected. The value of L_{b1} and L_{b2} are calculated in each mode as:

$$L_{b1}=\begin{cases} Mode1: & \dfrac{D\times V_{DC}}{\Delta i_{Lb1}\times f_s} \\ Mode2\&3: & \dfrac{(1-D)\times V_M}{\Delta i_{Lb1}\times f_s} \\ Mode4: & \dfrac{D\times V_M}{\Delta i_{Lb1}\times f_s} \\ Mode5: & \dfrac{(1-D)\times V_{DC}}{\Delta i_{Lb1}\times f_s} \end{cases} \quad (51)$$

$$L_{b2}=\begin{cases} Mode1\&4: & \dfrac{(1-D)\times V_B}{\Delta i_{Lb2}\times f_s} \\ Mode2\&3\&5: & \dfrac{D\times V_B}{\Delta i_{Lb2}\times f_s} \end{cases} \quad (52)$$

where Δi_{Lb1} and Δi_{Lb2} are the desired current ripple of L_{b1} and L_{b2}, respectively. According to the converter specifications the value of inductors in each operating mode should be calculated and the maximum of them should be selected. The value of the Lb3 can be calculated using below equation too:

$$L_{b3}=\frac{V_{FC}*D}{\Delta i_{Lb3}*f_s} \quad (53)$$

The C_{b1} can be sized using average current of L_{b2} (i_{Lb2}) as follows:

$$C_{b1} = \frac{i_{Lb2} \times (1-D)}{\Delta v_{Cb1} \times f_s} \quad (54)$$

where Δv_{Cb1} is the voltage ripple of the C_{b1}. The same approach can be used in order to obtain the value of C_{b3}.

Control Method

Since the proposed converter charges the battery via the grid in mode1 and returns the battery energy to grid during mode5, the power quality issues should be considered. The input current waveform in terms of THD and the power factor, are the main factors of a grid-connected converters which should be designed correctly. The proposed converter has the ability to work as a converter with power factor correction (PFC) and a converter with controllable absorbed and generated active and reactive power during mode1 and mode5, respectively, according to the processed smart grid commands or costumer requirements. This feature enables the grid operator to control connected converters during peak hours. In both aforementioned conditions an appropriate control method is needed to control the AC-DC stage and input current THD, simultaneously. Since the proposed converter is a two-stage one, each stage needs separated controllers which can work dependently or independently. For controlling both active and reactive power the controllers should work dependently in order to have constant voltage in the battery port. Proportional-Integral (PI) control is a very simple and robust method for controlling power converters. A very effective dual-loop PI controller is designed and adopted for the AC-DC stage in this paper. The first loop of the proposed controller consists of active and reactive control loops (P and Q loops) which control the used or injected P and Q powers according to the commands which are defined by costumer or smart grid by calculating reference input current. The second loop controls the input current according to the reference calculated by the previous loop by generating Sa1~Sa4 gate pulses. The operation of the proposed five-step dual-loop control method is detailed in this section. In the first step two delay blocks are used to generate the quadrature signals of the grid voltage and input current Fig. 12.

If the sampling frequency assumed 20kHz, one quarter delay leads to 100 samples (1/4*50). In the next step, the instantaneous pq theory introduced in [24] is used to calculate the single-phase P and Q power as illustrated in Fig. 12. In the third step, the calculated active and reactive power are used in the P and Q loops, respectively, in order to obtain references of active and reactive power. As depicted in Fig. 13, the P-loop controls active power by controlling DC-link voltage. At first, the error signal between calculated active power (P) and active power command (P_c) is fed to the primary PI controller which generates DC-link voltage reference ($V_{DC,ref}$). The secondary PI controller is used to calculate active power reference (P_{ref}) using error signal between measured and reference of the DC-link voltage. In the Q-loop, a PI controller is used to calculate reactive power reference according to the reactive power command (Q_c). It is worth mentioning that it is possible to control the DC-link voltage directly by defining $V_{DC,ref}$ by the costumer according to the grid and converter properties and battery voltage. Clearly in this condition only the reactive power can be controlled. In order to clarify the charging and discharging strategy, the control method selection process is illustrated in Fig. 14.

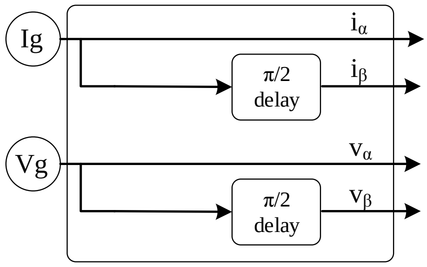

Fig. 11: First step of control method: calculating quadrature signals.

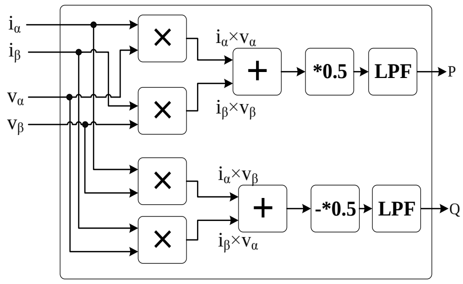

Fig. 12: Second step of control method: calculating active and reactive power.

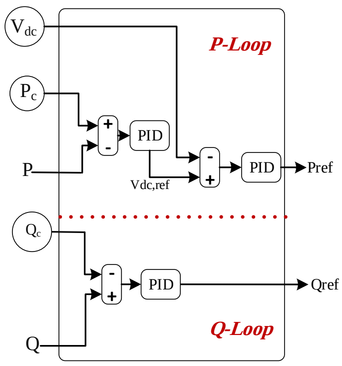

Fig. 13: third step of control method: calculating active and reactive power references.

In the fourth step, the input current reference (I_{ref}) is obtained by using the generated active and reactive power references and (55)-(57) equations as follows:

$$\theta = \tan^{-1}(\frac{Q_{ref}}{P_{ref}}) \tag{55}$$

$$I_{ref} = \frac{P_{ref}}{V_g \operatorname{Cos}(\theta)} \tag{56}$$

$$i_{ref}^{*} = \sqrt{2} I_{ref} \operatorname{Sin}(w_t - \theta) \tag{57}$$

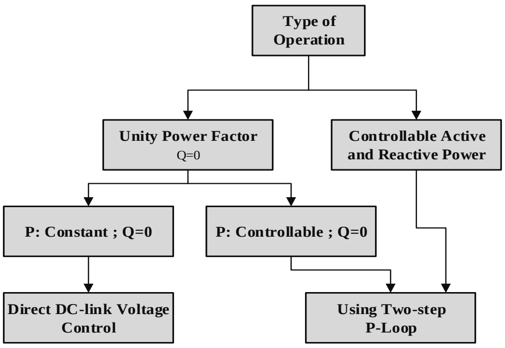

Fig. 14: Procedure of controller method selection.

In the last step the Sa1~Sa4 gate pulses are generated by using a PI controller, a comparator, and logic functions as shown in Fig. 15. At first error signal between measured and reference of input current signal is fed to a PI controller and then the output of that is compared with a high frequency (20-30 kHz) triangular wave. Finally logic functions are used to generate gate pulses.

Comparison Study

The proposed converter is compared with similar converters introduced in recent years in term of operating modes that they can work in and high frequency switches in each mode and results are provided in Table 1. At first blush, existence of 4 switches in the AC-DC stage and 7 switches in the DC-DC stage might come across as a cause of significant power loss in the circuit, but it is notable that there are not more than 4 high frequency switches in each mode.

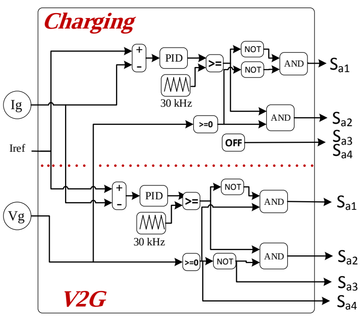

Fig. 15: last step of control method: generating gate pulses.

As explained in Table 1, the proposed converter is capable of working in five operating modes in buck-boost condition with less or equal number of high frequency switches in comparison of other converters, which is an impressive feature of that. The capacity of each component and cost analysis of the presented converter is indicated in Table 2. Two converters with 2kW and 5kW power are assumed and model and cost of each element are analyzed. Like other two-stage converters, DC-link capacitor increases the cost and volume of the converter. It should be noted that the analyzed converter is the main and only power circuit in a PHEV and there is no need for additional power circuit.

Simulation Results

The simulation of the proposed converter has been done in MATLAB/SIMULINK environment and results are provided in this section. The properties of the simulated system are tabulated in Table 3. The minimum values of passive components can be calculated according to the above-mentioned design considerations. The values of L_a, L_{b1}, L_{b2}, and L_{b3} can be obtained by using (46), (51), (52), and (53), respectively. (49) and (54) are used to calculate the minimum values of capacitors. The second control method (V_{DC} direct control) with unity power factor is selected for controlling AC-DC stage and the DC-DC stage is simulated open loop. Different DC-link, battery port, and motor voltages are selected during simulation in order to emphasize the buck-boost operation of the proposed converter. The power of battery and motor are assumed 5kW.

Table 1: Operating modes comparison of proposed converter with other presented converters

Reference	Number of high frequency switch(s) in :				
	Mode1	Mode2	Mode3	Mode4	Mode5
[10]	×	6 (Boost)	×	6 (Buck)	×
[11]	×	4 (Boost)	×	4 (Buck)	×
[12]	×	×	4 (Boost)	×	×
[13]	×	×	4 (Boost)	4 (Buck)	×
[14]	×	2 BB	4 BB	4 BB	×
[15]	×	2 BB	4 BB	4 BB	×
[16]	2 (Boost)	3 BB	×	3 BB	×
[17]	4 BB	1 (Boost)	×	1 (Buck)	×
[18]	4 BB	×	×	×	×
[19]	2 BB	2 BB	×	2 BB	×
[20]	3 (Buck)	×	×	×	5 (Boost)
Proposed Converter	4 BB	2 BB	4 BB	2 BB	4 BB

- BB: Buck-Boost

Table 2: Cost Analysis of the proposed converter

Component	2kW Parameters	5kW Parameters	2kW Cost	5kw Cost
AC-DC Stage Switches	4*TTKK2837 (24A;500V)	4*FGW40N120HD (40A;1200V)	4*(1.01$)=4.05$	4*(0.86$)=3.46$
DC-DC Stage Switches	5*KF13N60(13A;600V) 2*FGW40N120HD (40A;1200V)	3*FGW40N120HD(40A;1200V) 3*GT30J122A(30A;600V) 1*KF130N60(13A;600V)	5*(0.36$)+2*(0.86$)=3.52$	3*(0.86$)+3*(0.8$)+1*(0.36$)=5.34$
Diode (Db6)	30eth06(30a;600v)		0.62$	
Inductors	core and wire		11.5$	13$
DC-Link Capacitor (Ca)	6*(1360µF;450V)		6*(2.72$)=16.3$	
Cb1	4*(470µF;450V)		4*1.5$=6$	
Cb2	1*(470µF;250V)		0.95$	
Cb3	1*(470µF;250V)		0.78$	
CM	4*(560µF;450V)		4*1.5$=6$	

The presented converter is simulated in mode1 with VB=240V and input current and grid voltage are shown in Fig. 15 and as can be seen the power factor is more than 0.99. Fig. 16 shows the FFT analysis of the input current over 3 cycles which is 4.43%. The perfect ability of the converter to track the reference input current generated by the controller is illustrated in Fig. 17.

Table 3: The Proposed Converter Specifications

	Simulation	Experimental
AC Input Voltage	220 (RMS)	36 (RMS)
DC –Link Voltage	350 V	110,90 V
FC Voltage	150 V	20 V
L_a	6 mH	4 mH
L_{b1},L_{b2}	5 mH	1.5 mH
L_{b3}	1.2 mH	1.5 mH
C_a	10 mF	4 mF
C_{b1}	500 uF	1000 uF
C_{b2}	470 uF	680 uF
C_{b3}	120 uF	1000 uF
C_M	470 uF	680 uF
AC Input Frequency	50 Hz	50 Hz
Switching Frequency	30 kHz	25-30 kHz
Power Factor	0.99	0.99
Controller	-	ARMSTM32F103RET
Mosfet	-	KF13N60
Current Sensor	-	ACS712

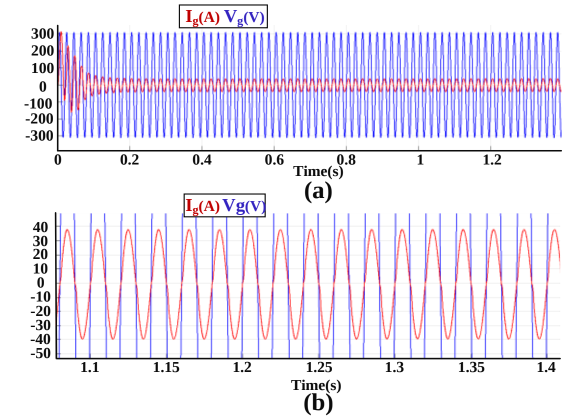

Fig. 16: (a) grid voltage and input current in mode1 (b) enlarged version

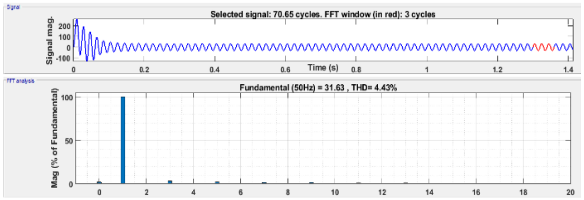

Fig. 17: FFT analysis of input current in mode1

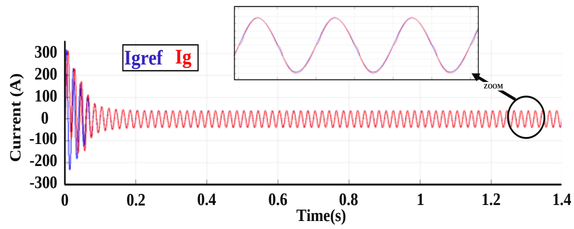

Fig. 18: Reference and measured input current in mode1.

As shown in Fig. 19, the DC-link and battery port voltages have very fast transient and acceptable steady-state ripple.

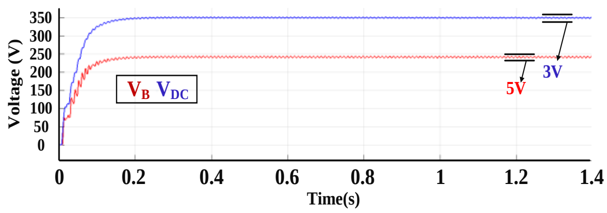

Fig. 19: DC-link and battery port voltages in mode1.

Voltage and current of L_{b1}, L_{b2}, and C_{b1} in each time intervals are shown Fig. 20 through Fig. 22, respectively.

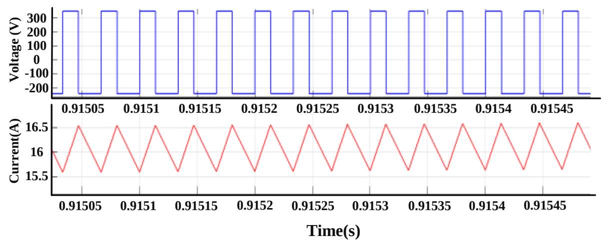

Fig. 20: voltage and current of Lb1 in mode1.

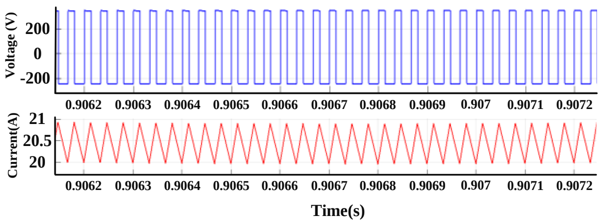

Fig. 21: voltage and current of Lb2 in mode1.

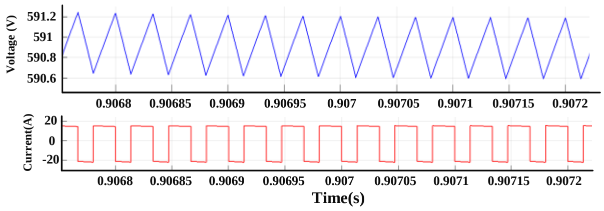

Fig. 22: voltage and current of Cb1 in mode1.

The second mode is simulated with V_B=240V and V_M=600V and results are shown in Fig. 23.

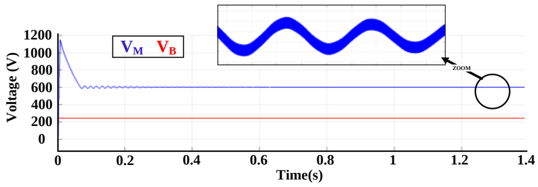

Fig. 23: Battery port and motor voltages in mode2.

The motor voltage in different conditions (in terms of battery and FC voltage) for various duty cycles is illustrated in Fig. 24.

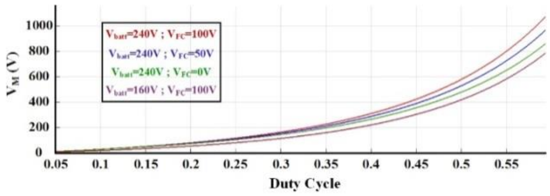

Fig. 24: Motor voltage in different conditions

Fig. 25 shows the transient of the motor voltage during switching between mode2 and mode3. At t=0.6s FC starts working and at t=1.5s finishes. As can be seen, the V_M is fixed on 600V in its steady-state. The gate pulses of Sb2, Sb3, Sb6, and Sb7 are shown in Fig. 26.

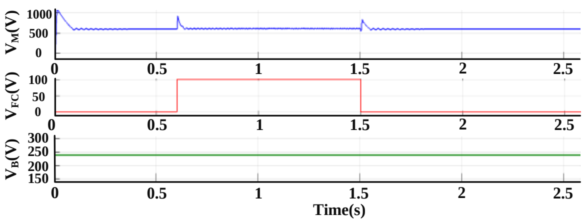

Fig. 25: VM, VFC, and VB during switching between mode2 and mode3.

Fig. 27 shows the motor voltage and battery port voltage during braking condition (Mode4). In order to validate buck-boost operation of the proposed converter the motor voltage is decreased in three steps but battery port voltage is fixed on 240V.

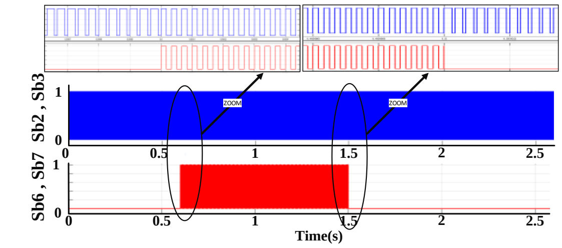

Fig. 26: Gate pulses of Sb2, Sb3, Sb6, and Sb7 during switching between mode2 and mode3.

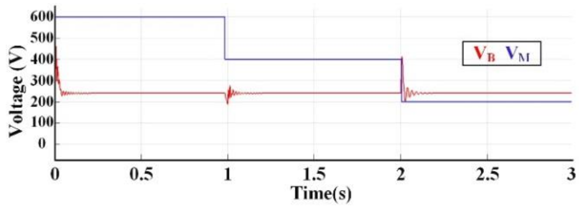

Fig. 27: motor and battery port voltage in mode4.

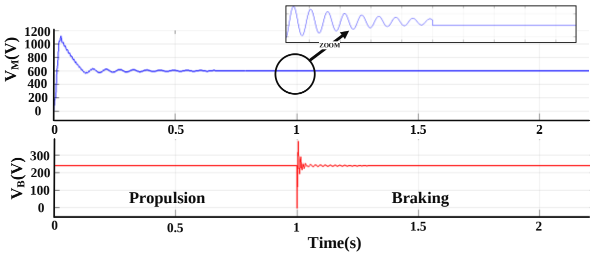

Fig. 28: Battery and motor voltages during switching between propulsion and braking modes.

In order to analyze the dynamic response of the converter during braking times, the proposed converter is simulated during switching between propulsion and braking modes and results are shown in Fig. 28. It is assumed that the vehicle starts braking at t=1s.

The V2G mode (Mode5) is also simulated. Fig. 29 shows grid voltage and input current in mode5 and FFT analysis of input current is depicted in Fig. 30.

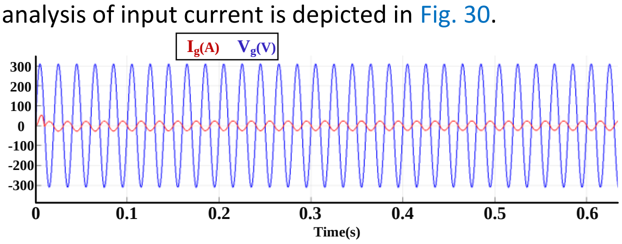

Fig. 29: grid voltage and input current in mode5.

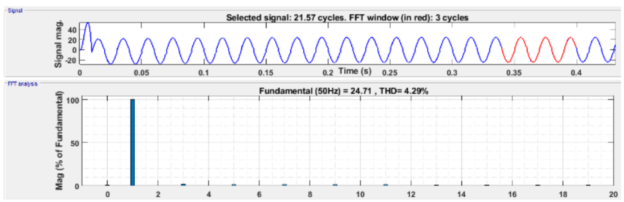

Fig. 30: FFT analysis of input current in mode5

Experimental Verification

A reduced-scale prototype of proposed converter has been built and experimental results are provided in order to verify simulation ones. Fig. 31 shows the experimental setup with specifications tabulated in Table 3. It is worth mentioning that the value of parameters are obtained using the aforementioned design considerations. Similar to simulation, the prototype is controlled and tested in UPF condition during mode1. In order to compare experimental results with simulation ones, the proposed converter is simulated again with experimental parameters and result are provided in this section.

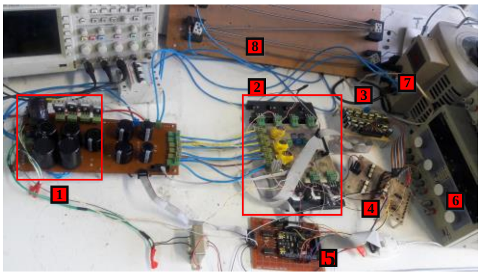

1- AC-DC Stage
2- DC-DC Stage
3- Isolated gate drive supply
4- Gate driver board
5- Control board (STM32F103RET)
6- ACS712 and op-amps supply
7- Autotransformer
8- Load

Fig. 31: Implemented system.

Fig. 32 shows grid voltage and input current during mode1 which have unity power factor. Fig. 32 (c) shows converter behavior during battery power changing from 250W to 150W. In order to test buck and boost operation of DC-DC stage, mode1 is tested under two conditions, (V_{DC}=110V, V_B=80V, P_B=250W) and (V_{DC}=90V, V_B=120V, P_B=250W) and results are shown in Fig. 33.

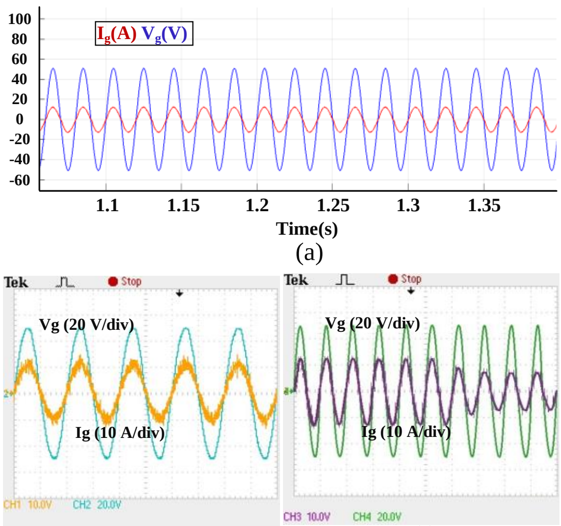

(a)

(b) (c)

Fig. 32: grid voltage and input current in mode1; Simulation: (a) PB=250W; Experimental: (b) PB=250W (c) PB decreases from 250W to 150W.

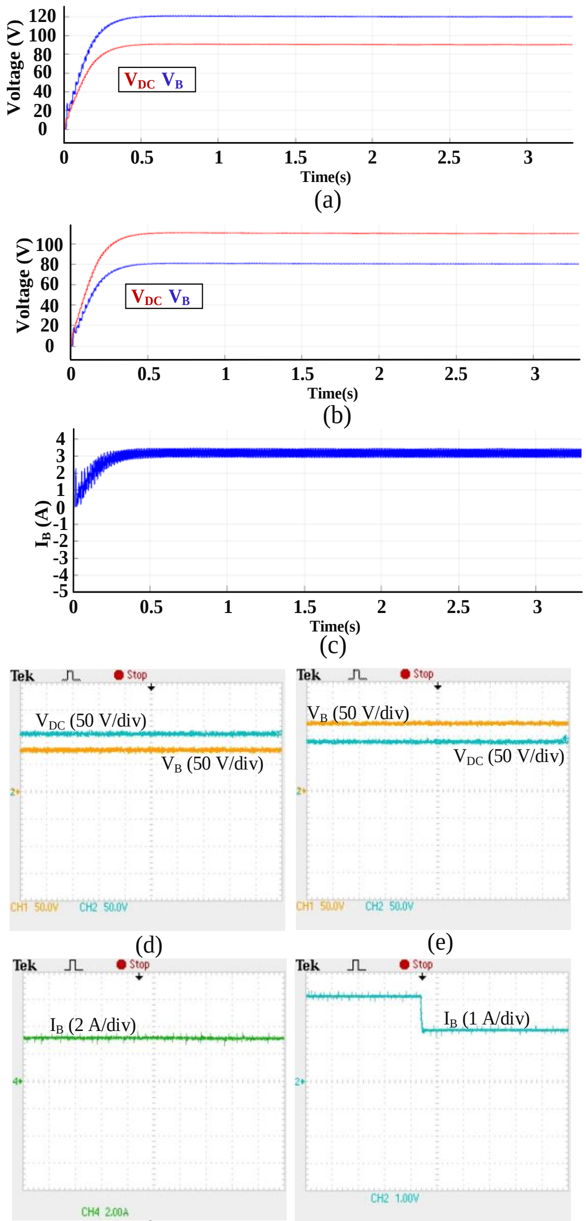

(a) (b) (c) (d) (e) (f) (g)

Fig. 33: Simulation: DC-link and battery port voltage during mode1 in (a) boost condition (b) buck condition (c) battery current in buck condition; Experimental: DC-link and battery port voltage during mode1 in (d) buck condition (e) boost condition (f) battery current (PB=250W) (g) battery current (PB decreases from 250W to 150W) in buck condition.

The converter is tested during mode2 with V_B=80V and V_M=120V; P_M=250W. Fig. 34 shows the voltage and current of the battery and motor ports in this mode. Voltage and current of L_{b1} and L_{b2} are depicted in Fig. 35. The converter is operated in mode3 in order to feed the 250W motor port and Fig. 36 shows the FC, battery, and motor voltage during this mode.

The braking mode (mode4) is tested under two conditions: V_M=120V and V_M=70V with V_B=80V; P_B=250W and results are depicted in Fig. 37.

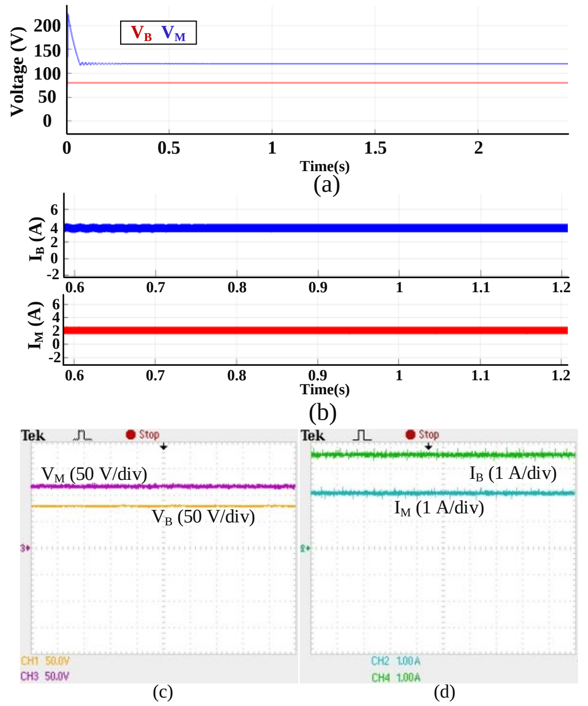

Fig. 34: Simulation: (a) Battery port and motor voltage in mode2 (b) Battery port and motor current in mode2; Experimental: (c) Battery port and motor voltage in mode2 (d) Battery port and motor current in mode2.

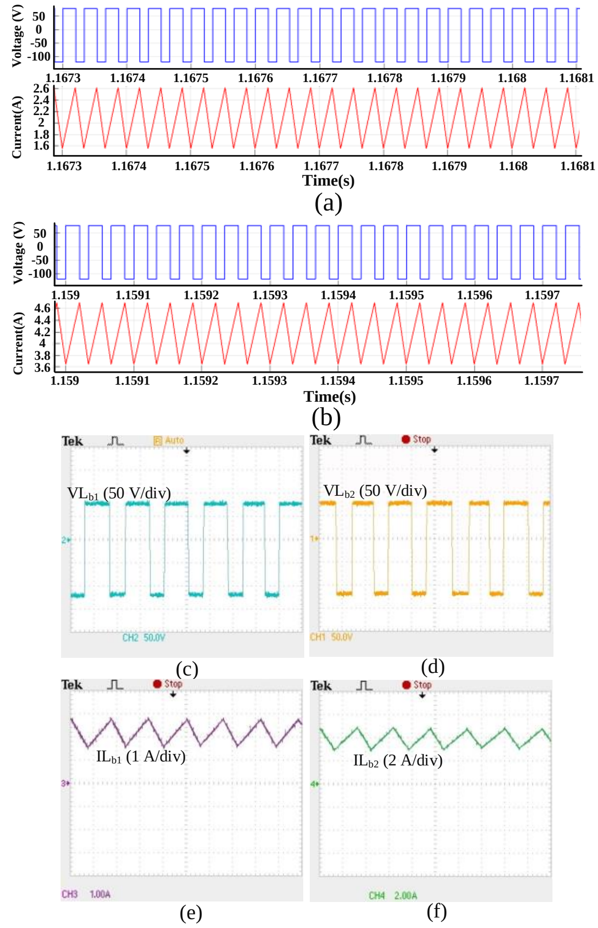

Fig. 35: Simulation: voltage and current of (a) Lb1 (b) Lb2; Experimental: voltage across (c) Lb1 (d) Lb2, current of (e) Lb1 (f) Lb2 during mode2.

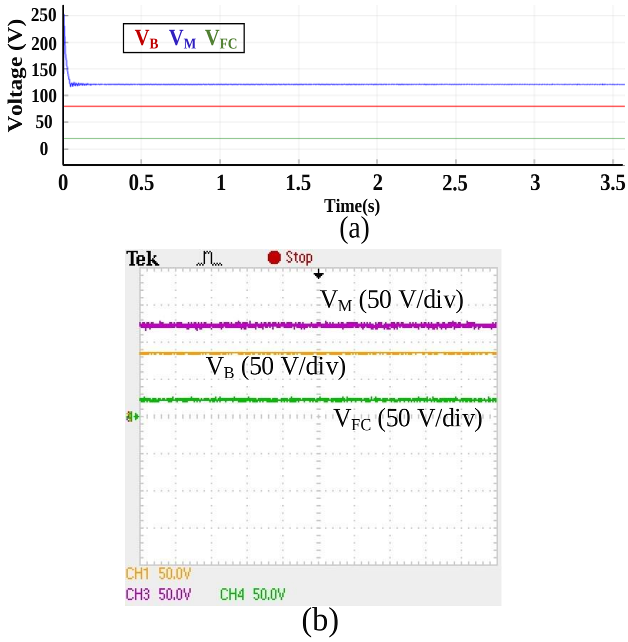

Fig. 36: (a) Simulation results (b) experimental results of FC, battery, and motor voltages during mode3.

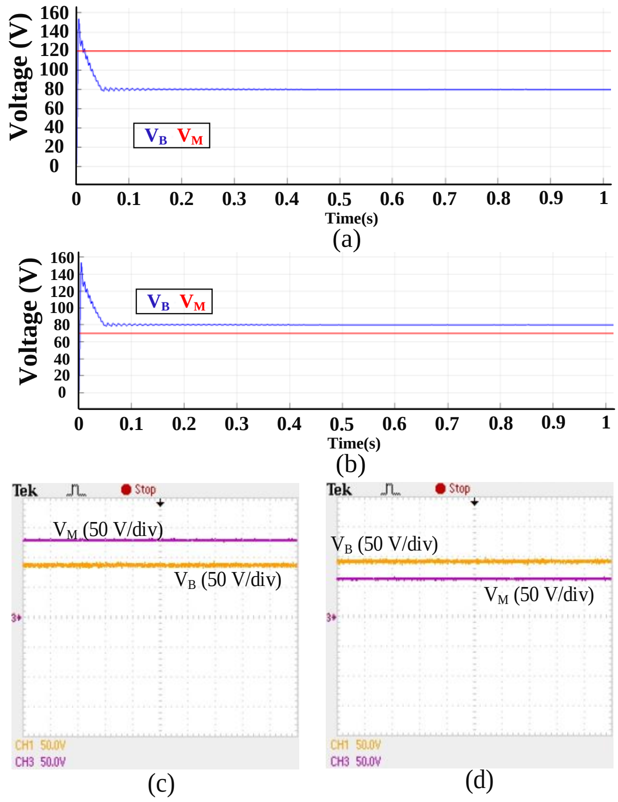

Fig. 37: Simulation: battery and motor voltages (a) buck (b) boost condition; Experimental: battery and motor voltages (c) buck (d) boost condition during mode4

Vehicle to grid mode is also tested and results are shown in Fig. 38.

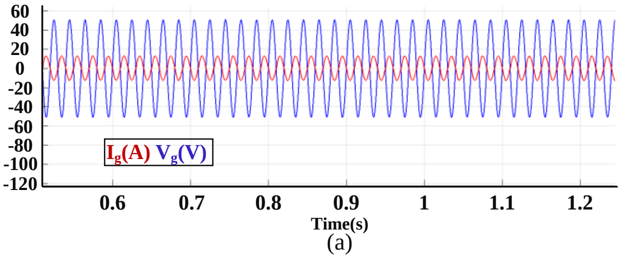

(a)

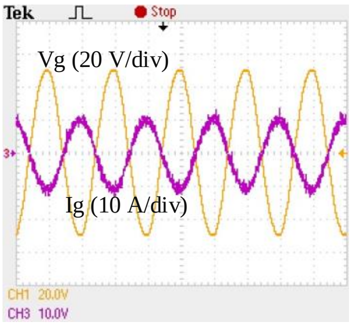

(b)

Fig. 38: (a) Simulation (b) Experimental results of grid voltage and input current during mode5.

Results and Discussion

The proposed converter is simulated in MATLAB/SIMULINK software in all operating modes. Current and voltage waveforms with their transient and steady state in all operating conditions are provided in order to confirm its perfect ability to track references (voltage and current) in terms of dynamic response and steady state ripple. The power factor and THD of the input current is also analyzed which shows its unity power factor and acceptable current THD (less than 5%) in the operating modes in which the grid works as a power source. In order to show the converter behavior during modes switching and voltages changing, it is simulated in different conditions. An experimental prototype is also implemented and experimental results are provided in all operating modes. As shown in figures, the input current has acceptable THD (less than 5%) and converter power factor is more than 0.9. In order to compare experimental results with simulation ones, the converter is also simulated with experimental parameters and results are provided.

Conclusion

A bidirectional buck-boost integrated converter has been introduced in this paper. The proposed converter can be used in PHEVs which use battery and FC as power sources and is capable of working in five different operating modes which have been explained and analyzed in detail in this paper. The design procedure of the presented converter is provided and also an effective control method to control active and reactive power during charging and V2G modes is introduced. The proposed converter is also compared with other similar converters introduced in recent years in terms of number of high frequency switches in each mode. The simulation of the presented converter is done in MATLAB/SIMULINK in order to validate system analysis. An experimental prototype of the converter has been built and tested and experimental results are provided.

Author Contributions

H. Soltani Gohari designed, analyzed, simulated, implemented the system, and wrote the manuscript. K. Abbaszadeh carried out the supervision.

Acknowledgment

This work is partially supported by grant from K.N.Toosi University of Technology.

Conflict of Interest

The author declares that there is no conflict of interests regarding the publication of this manuscript. In addition, the ethical issues, including plagiarism, informed consent, misconduct, data fabrication and/or falsification, double publication and/or submission, and redundancy have been completely observed by the authors.

References

[1] A. Khaligh, M. D'Antonio, "Global trends in high-power on-board chargers for electric vehicles," IEEE Transactions on Vehicular Technology, 68(4): 3306-3324, 2019.

[2] H. V. Nguyen, D.-D. To, D.-C. Lee, "Onboard battery chargers for plug-in electric vehicles with dual functional circuit for low-voltage battery charging and active power decoupling," IEEE Access, 6: 70212-70222, 2018.

[3] S. M. Lukic, A. Emadi, "Charging ahead," IEEE Industrial Electronics Magazine, 2(4): 22-31, 2008.

[4] C. C. Chan, "The state of the art of electric, hybrid, and fuel cell vehicles," in Proceedings of the IEEE, 95(4): 704-718, 2007.

[5] I. Aharon, A. Kuperman, "Topological overview of powertrains for battery-powered vehicles with range extenders," IEEE Transactions on Power Electronics, 26(3): 868-876, 2011.

[6] W. Qian, H. Cha, F. Z. Peng, L. M. Tolbert, "55-kW variable 3X DC-DC converter for plug-in hybrid electric vehicles," IEEE Transactions on Power Electronics, 27(4): 1668-1678, 2011.

[7] T. Park, T. Kim, "Novel energy conversion system based on a multimode single-leg power converter," IEEE transactions on power electronics, 28(1): 213-220, 2012.

[8] H. Bai, Y. Zhang, C. Semanson, C. Luo, C. Mi, "Modelling, design and optimisation of a battery charger for plug-in hybrid electric vehicles," IET electrical systems in transportation, 1(1): 3-10, 2011.

[9] J.-S. Kim, G.-Y. Choe, H.-M. Jung, B.-K. Lee, Y.-J. Cho, K.-B. Han, "Design and implementation of a high-efficiency on-board battery charger for electric vehicles with frequency control strategy," in IEEE Vehicle Power and Propulsion Conference,:1-6, 2010.

[10] N. Elsayad, H. Moradisizkoohi, O. A. Mohammed, "A New Hybrid Structure of a Bidirectional DC-DC Converter With High Conversion Ratios for Electric Vehicles," IEEE Transactions on Vehicular Technology, 69(1): 194-206, 2019.

[11] Y. Zhang, Y. Gao, L. Zhou, M. Sumner, "A switched-capacitor bidirectional DC–DC converter with wide voltage gain range for electric vehicles with hybrid energy sources," IEEE Transactions on Power Electronics, 33(11): 9459-9469, 2018.

[12] R. R. Ahrabi, H. Ardi, M. Elmi, A. Ajami, "A novel step-up multiinput DC–DC converter for hybrid electric vehicles application," IEEE Transactions on Power Electronics, 32(5): 3549-3561, 2016.

[13] H. Moradisizkoohi, N. Elsayad, O. A. Mohammed, "Experimental Verification of a Double-Input Soft-Switched DC–DC Converter for Fuel Cell Electric Vehicle With Hybrid Energy Storage System," IEEE Transactions on Industry Applications, 55(6): 6451-6465, 2019.

[14] F. Akar, Y. Tavlasoglu, E. Ugur, B. Vural, I. Aksoy, "A bidirectional nonisolated multi-input DC–DC converter for hybrid energy storage systems in electric vehicles," IEEE Transactions on Vehicular Technology, 65(10): 7944-7955, 2015.

[15] C.-M. Lai, Y.-H. Cheng, M.-H. Hsieh, Y.-C. Lin, "Development of a bidirectional DC/DC converter with dual-battery energy storage for hybrid electric vehicle system," IEEE Transactions on Vehicular Technology, 67(2): 1036-1052, 2017.

[16] S. Dusmez, A. Khaligh, "A compact and integrated multifunctional power electronic interface for plug-in electric vehicles," IEEE Transactions on Power Electronics, 28(12): 5690-5701, 2012.

[17] S. Dusmez, A. Khaligh, "A charge-nonlinear-carrier-controlled reduced-part single-stage integrated power electronics interface for automotive applications," IEEE transactions on Vehicular Technology, 63(3): 1091-1103, 2013.

[18] Y. Tang, D. Zhu, C. Jin, P. Wang, F. Blaabjerg, "A three-level quasi-two-stage single-phase PFC converter with flexible output voltage and improved conversion efficiency," IEEE Transactions on Power Electronics, 30(2): 717-726, 2014.

[19] A. K. Singh, M. K. Pathak, "Single-stage ZETA-SEPIC-based multifunctional integrated converter for plug-in electric vehicles," IET Electrical Systems in Transportation, 8(2): 101-111, 2017.

[20] S. Liu, X. Xie, L. Yang, "Analysis, Modeling and Implementation of a Switching Bi-Directional Buck-Boost Converter Based on Electric Vehicle Hybrid Energy Storage for V2G System," IEEE Access, 8: 65868-65879, 2020.

[21] H. S. Gohari, K. Abbaszadeh, "A Novel Controllable Bidirectional switching-capacitor based Buck-Boost Charger for EVs," in 2020 11th Power Electronics, Drive Systems, and Technologies Conference (PEDSTC),:1-6, 2020.

[22] V. Bist, B. Singh, "PFC Cuk converter-fed BLDC motor drive," IEEE Transactions on Power Electronics, 30(2): 871-887, 2014.

[23] V. Vlatkovic, D. Borojevic, F. C. Lee, "Input filter design for power factor correction circuits," IEEE Transactions on Power Electronics, 11(1): 199-205, 1996.

[24] H. Akagi, Y. Kanazawa, A. Nabae, "Instantaneous reactive power compensators comprising switching devices without energy storage components," IEEE Transactions on industry applications(3): 625-630, 1984.

Biographies

Homayon Soltani Gohari received the B.Sc. degree in electrical power engineering from Shahid Bahonar University of Kerman, Kerman, Iran, in 2017 and M.Sc. degree in electrical power engineering, Power electronics, from K.N.Toosi University of Technology, Tehran, Iran, in 2020. His research field includes power electronics, EVs power converter, energy management, and different power converters especially rectifiers with PFC.

Karim Abbaszadeh received the B.S. degree in communication engineering from Khajeh Nasir Toosi University of Technology, Tehran, Iran, in 1991, and the M.S. and Ph.D. degrees in electrical engineering from Amir Kabir University of Technology, Tehran, Iran, in 1997 and 2000, respectively, from 2001 to 2003, he was a Research Assistant with the Department of Electrical Engineering, Texas A&M University, College Station, TX, USA. He is currently a Professor with the Department of Electrical Engineering, Khajeh Nasir Toosi University of Technology. His research interests include power electronic and dc–dc and dc–ac converters, electric machinery, variable-speed drives, and propulsion applications. He is the author of more than 50 published journal papers. He is actively involved in presenting short courses and consulting in his area of expertise to various industries.

How to cite this paper:
H. Soltani Gohari, K. Abbaszadeh, “Bidirectional Buck-Boost Integrated Converter for Plug-in Hybrid Electric Vehicles” Journal of Electrical and Computer Engineering Innovations, 8(1): 109-124, 2020.

DOI: 10.22061/JECEI.2020.7076.354

URL: http://jecei.sru.ac.ir/article_1431.html